UNIVERSITY "POLITEHNICA" OF BUCHAREST

Faculty of Chemical Engineering and Biotechnologies

The use of renewable raw materials to obtain high-performance products

PhD Thesis Summary

Professor superviser:

Prof. Dr. Ing. Raluca STAN

Author:

Raluca Sanda AELENII (KOMARTIN)

Bucharest

2022

In memory of my parents who made me who I am and who would have so much enjoyed this moment.

Content of PhD Thesis Summary

1. INTRODUCTION

In this work we aimed to obtain new products using renewable materials, mainly *Lallemantia iberica* oil (LALO). This less-known oil, displaying a higher degree of unsaturation than linseed oil, proved to have remarkable potential application.

We also used lignin as a second bio-based component, a very abundant, sustainable natural material, with a positive carbon footprint and a versatile chemistry. Until recently, in form of fractionated or functionalized versions, lignin was not available in large quantities. However, industrial processes for its isolation and purification, as well as chemical modification, have opened up a multitude of interesting applications.

Lallemantia iberica, an annual oil plant native to Siberia and the Himalayas, spread throughout the rest of Asia and Europe. In some countries such as Iran, Egypt, Turkey it is used as a common annual crop, with seeds mainly used for traditional medical and food purposes. The whole plant is a source of aromatic essential oils, which are obtained by steam distillation. These oils consist mainly of volatile terpenes and should not be confused with the non-volatile triglyceride oil from the seeds. In many parts of the world the *Lallemantia* plant also appears as a decorative garden plant.

Cultivated in the past on a large scale in Ukraine, Moldavia and Russia, *Lallemantia* provided an edible oil known as "the oil of the poor" because it had a bitter taste. In this use, however, it was gradually replaced later by sunflower oil. Surprisingly, in spite of being more unsaturated than linseed oil (LO), *Lallemantia iberica* oil (LALO) is more storage-stable than the former one. We should also mention that LALO obtained by modern processes has superior organoleptic properties, which gives it an advantage over linseed oil, which has a rather unpleasant taste.

Although no industrial applications have yet appeared in Europe or the USA, there is an increased interest in the cultivation of the *Lallemantia iberica* plant and in the properties of its oil, as reflected in various publications [1-6]. Currently, small amounts of LALO are offered on the internet at a high price.

As we are going to show below, there are serious arguments pointing to the interest of a large-scale activity around this "forgotten" oilseed plant, which has the potential of creating new sectors of economic activity. As compared to current oils, the *Lallemantia* oil stands out by its unusually high proportion of polyunsaturated acids, with obvious advantages for food applications and for use as starting material for performant industrial products.

2. OBJECTIVES

The objectives of this work were:

- The use of two performing oils, one less known, LALO, and another similar to it, the well-known linseed oil (LO).
- Development of an optimized method for obtaining LALO from seeds, since this oil is not yet industrially available.
- Elaboration of a preliminary laboratory treatment to make the oil suitable for further functionalization.
- LALO functionalization by introducing an oxirane group (epoxidation), in order to confer it a special reactivity and to make it convenient as a raw material (ELALO) for thermoplastic polymers.
- The use of epoxidized linseed oil (ELO) for comparison, with well-known performance in the literature and in industrial practice.
- Preparation of epoxy resins starting from ELALO and ELO.
- The use of these resins as matrices for composites, incorporating as filler lignin, either unmodified (LnK) or as an epoxidized derivative (ELnK).
- Preparation of anticorrosive coatings, as an application of ELO-LnK composites.
- Preparation of composite materials based on ELALO-ELnK.
- The use of structure directing agents (SDA) for better lignin dispersion in ELALO-ELnK composites.
- Thermal and structural characterization of the obtained composites.

The achievement of these objectives materialized in the following steps:

Oil extraction from Lallemantia iberica seeds, extraction optimization, pre-treatment and characterization of the obtained oil.

- Obtaining the oil by extraction from the seeds of *Lallemantia iberica*.
- Selection of the best-suited extraction method.
- Determination of optimized extraction parameters, using the response surface methodology (RSM).
- Refining the obtained LALO to make it suitable for derivatization (epoxidation).
- Characterization of LALO.

Preliminary studies to obtain composites based on ELALO and ELO using lignin as filler.

- Identification of crosslinking possibilities and adequate reaction conditions for ELALO and ELO.

- Preparation of composites based on ELALO and ELO using kraft lignin (LnK) for reinforcement, either unmodified or functionalized by epoxidation (ELnK).

The use of non-functionalized lignin (LnK) in an ELO-based polymer used for corrosion protection.

- Preparation of ELO-LnK composites and their characterization by FTIR, TGA, DMA, CA, WAD and SEM.
- The use of the resin as coating on carbon steel plates and testing it for anticorrosion performance.

The use of epoxidized lignin (ELnK) in an ELALO-based polymer for various types of applications.

- Preparation of ELALO-ELnK composites using different SDAs.
- Characterization of ELALO-ELnK composites by FTIR, TGA, DMA, CA, WAD and SEM.

3. CONTENT

4. SUMMARY – ORIGINAL CONTRIBUTIONS

CHAPTER IV. Obtention of *Lallemantia iberica* oil, optimization of extraction and treatment

4.1. EXTRACTION OF OIL FROM *LALLEMANTIA* SEEDS

The Soxhlet type extraction was first chosen, this being considered one of the methods that ensures the highest yield. This was also the reason why the Soxhlet extraction was chosen as reference in the extraction optimization process and part of the oil yield calculation formula (the oil yield of the Soxhlet extraction was used as theoretical quantity in the yield formula, the yield being the dependent variable in the optimization equation).

The yield formula was (4.1):

$$\eta\ (\%) = \frac{oil\ quantity\ (g)}{m_{oil\ Soxhlet\ (g)}} \cdot 100 \qquad (4.1)$$

where: η (%) = yield of oil;

oil quantity = oil amount (g) extracted;

$m_{oil\ Soxhlet}$ = oil amount (g) by Soxhlet extraction using petroleum ether (=40.95 g) as a solvent.

The amount of oil corresponding to the calculated yield (with the optimization equation) and to the experimental yield (RSM method) was calculated using the above formula.

In order to choose the suitable solvent, the contribution of the following two factors was investigated: 1) the extractive capacity and 2) the quality of the obtained oil, as evaluated by the fatty acid profile determined by gas chromatography (GC). ***Tables 4.1.*** and ***4.2.*** show the values obtained for both monitored factors, in all three cases, the Soxhlet extractions with the three solvents (ethyl ether, petroleum ether and n-hexane). The values obtained are very close. If we consider economic factors, the prefered solvent is petroleum ether, which presents a volatility compromise (b.p. 40-60°C) compared to ethyl ether (b.p. 33°C) and n-hexane (b.p. 84°C). The results (*oil content* – in g oil/100 g seeds) were calculated with the following formula (4.2):

$$U\ (\%) = \frac{m_{oil\ (g)}}{m_{seeds\ (g)}} \cdot 100 \qquad (4.2)$$

where: U (%) = oil content of seeds;

m_{oil} = oil quantity (g) extracted;

m_{seeds} = seeds quantity (g) subjected to extraction.

Table 4.1. shows the oil quantity obtained after evaporation of solvents.

Table 4.1. Oil quantity

Solvents	***Oil (g/100 g seeds)***
n-Hexane (H)	40.2
Ethyl ether (EE)	40.5
Petroleum ether (EP)	41.0

Table 4.2. shows the fatty acid profile of the oil obtained from *Lallemantia* seeds for all three Soxhlet extractions with ethyl ether, petroleum ether and n-hexane.

Table 4.2. Fatty acid profile of oil obtained from Lallemantia iberica seeds

Peak	***Acid methyl ester***	***No. of C atoms and double bonds***	***Composition (mol %)***			***Mean values***	***Standard deviation***
			Ethyl ether				
1	Palmitic	C16-0	7.41	7.34	7.33	**7.36**	0.04
2	Palmitoleic (9 cis Hexadecenoic)	C16-1	0.20	0.23	0.21	**0.21**	0.01
3	Stearic	C18-0	2.01	2.01	2.01	**2.01**	0.01
4	cis-9-Oleic	C18-1 cis 9	11.75	11.67	11.80	**11.74**	0.06
5	Linoleic	C18-2	13.59	13.68	13.72	**13.66**	0.07
6	Eicosanoic (Arachidic)	C20-0	0.25	0.25	0.28	**0.26**	0.02
7	Linolenic	C18-3	64.79	64.83	64.65	**64.75**	0.09
			Petroleum ether				
1	Palmitic	C16-0	7.32	7.45	7.41	**7.39**	0.07
2	Palmitoleic (9 cis Hexadecenoic)	C16-1	0.18	0.20	0.18	**0.19**	0.01
3	Stearic	C18-0	2.05	1.95	1.98	**1.99**	0.05
4	cis-9-Oleic	C18-1 cis 9	11.62	11.71	11.65	**11.66**	0.05
5	Linoleic	C18-2	13.42	13.52	13.45	**13.46**	0.05
6	Eicosanoic (Arachidic)	C20-0	0.43	0.45	0.53	**0.47**	0.05
7	Linolenic	C18-3	64.98	64.72	64.80	**64.83**	0.13
			n-Hexane				
1	Pentadecanoic	C16-1	0.93	0.00	0.00	**0.31**	0.54
2	Palmitic	C16-0	7.47	7.26	7.26	**7.33**	0.12
3	Palmitoleic (9 cis Hexadecenoic)	C16-1	0.21	0.16	0.15	**0.17**	0.03
4	Stearic	C18-0	1.99	1.96	1.88	**1.95**	0.06
5	cis-9-Oleic	C18-1 cis 9	11.95	11.62	11.56	**11.71**	0.21
6	Linoleic	C18-2	13.46	13.30	13.21	**13.33**	0.13
7	Eicosanoic (Arachidic)	C20-0	0.25	0.21	0.21	**0.22**	0.02
8	Linolenic	C18-3	63.73	65.49	65.73	**64.98**	1.09

4.2. OPTIMIZING THE OIL EXTRACTION PROCESS

As we showed in the literature chapter regarding optimization, the 3-factor Box-Behnken model was used in this study, since it is a more efficient model for the response surface methodology (RSM) than the central composite design or the complete three-level factorial models [32].

The steps followed in the optimization process were: 1) in some preliminary experiments, several extraction methods were tested (Soxhlet extraction – mentioned above, batch extraction – under mechanical stirring, ultrasound-assisted extraction), involving variable factors (solid/liquid ratio, temperature, extraction time, sonication amplitude) and their influence on oil yield; 2) following the decisions made in step one (the extraction method chosen, the factors identified as having a significant effect on the yield and their range of values), the factorial experiment itself was carried out. According to the Box-Behnken program for three factors and three levels, a number of 17 experiments, with 5 "at the center", were needed to determine method errors.

4.2.1. Preliminary experiments

The preliminary experiments had two goals: a) choosing the optimal extraction method for the factorial model and b) choosing the parameters (independent variables) according to which to vary the extraction conditions (their minimum, central and maximum values) fitting the extraction model. Based on these parameters the Box-Behnken experimental design matrix will be determined. The following preliminary experiments were performed:

- ***Extractions using an orbital shaker to determine:***

• the influence of the S/L ratio (1/8, 1/12, 1/16, 1/20) (extr. time 2h, temp. 25℃) – 4 experiments;

• the influence of extraction time (1,2,3,4h) (S/L=1/16, temp.25℃) – 4 experiments.

- ***Extractions using a simple reflux apparatus to determine:***

• the influence of temp. (25℃, 45℃) (S/L=1/20, extra time 3h) – 2 experiments.

- ***Ultrasound assisted extractions to determine:***

• the influence of the S/L ratio (1/16, 1/20) (extr. time 10 min, temp. 25-30℃, amplitude 30%) – 2 experiments;

• the influence of ultrasonic wave amplitude (20%, 40%) (extr. time 5min, temp. 25-30℃, S/L=1/16) – 2 experiments.

4.2.2. The factorial experiment

Following the preliminary experiments, the extraction method and 3 independent variables were selected: S/L ratio (X1), ultrasound amplitude (X2) and extraction time (X3). The second step of the optimization process consists in carrying out the actual factorial experiment.

Fitting the extraction model

The experimental design was done in terms of coded variables. There are mathematical reasons for this practice, but also a practical reason, namely that the design can be devised independently of the particular factors under study [31]. The three process parameters were varied between a maximum (+1), a minimum (-1) and a central (0) value, as can be seen in ***Table 4.8.***.

Table 4.8. Independent variables and the experimental field of Box-Behnken program

Independent variables		***Level***		
		-1	***0***	***1***
X1	S/L ratio, g/mL	***1:12***	***1:16***	***1:20***
X2	Ultrasound amplitude, %	***20***	***30***	***40***
X3	Extraction time, min	***5***	***10***	***15***

The Box-Behnken experimental matrix is presented in ***Table 4.9.*** in the form of coded values. ***Table 4.9.*** shows also the corresponding experimental and predicted values of the response variable (dependent variable).

Table 4.9. Experimental Box-Behnken matrix of independent variables and experimental and calculated values of extraction yield (Y)

Experiment No.	***S/L Ratio (X1)***	***Amplitude (X2)***	***Extraction Time (X3)***	***Experimental extraction yield***	***Predicted extraction yield***
0	**1**	**2**	**3**	**4**	**5**
E1	-1	-1	0	88.02	89.27
E2	1	-1	0	92.77	92.06
E3	-1	1	0	93.17	92.34
E4	1	1	0	94.84	95.13
E5	-1	0	-1	88.41	88.26
E6	1	0	-1	92.02	91.05
E7	-1	0	1	92.16	91.89
E8	1	0	1	93.30	94.68

E9	0	-1	-1	89.46	89.18
E10	0	1	-1	90.85	92.25
E11	0	-1	1	93.07	92.81
E12	0	1	1	96.73	95.88
E13	0	0	0	95.80	96.04
E14	0	0	0	96.59	96.04
E15	0	0	0	95.99	96.04
E16	0	0	0	95.85	96.04
E17	0	0	0	95.95	96.04

Experimental data were fitted using the following second-order polynomial regression model, which expresses the value of the dependent variable (***Y***) as a function of the three independent variables (***X_1, X_2, X_3***):

$$Y= a_0+a_1X_1+a_{11}X_1^2+a_2X_2+a_{22}X_2^2+a_3X_3+a_{33}X_3^2+a_{12}X_1X_2+a_{23}X_2X_3+a_{13}X_1X_3$$

where: a_0 – is the constant term of the polynomial; a_1, a_2, a_3 – are the linear coefficients; a_{11}, a_{22}, a_{33} – the quadratic coefficients and a_{12}, a_{13}, a_{23} – the interactive coefficients, respectively.

The STATISTICA 10 package software (Stat Soft Inc., Tulsa, USA) was used for data processing and experimental design analysis. Applying multiple regression analysis, the experimental data were used to calculate the coefficients of the second-order polynomial equation. Thus, considering only the relevant statistical terms, the equation obtained for the oil extraction yield (Y) is the following (4.4):

$$Y = 96{,}036 + 1{,}396\ X_1 - 2{,}445\ X_1^2 + 1{,}534\ X_2 - 1{,}39\ X_2^2 + 1{,}815\ X_3 - 2{,}118\ X_3^2 \quad (4.4)$$

The adequacy of the regression model was assessed by calculating R^2, the coefficient of determination, the value of which shows the extent to which the variability of the observed responses could be explained by the experimental factors and their interaction. The value of determination coefficient R^2 was 0.94, which indicates a good correlation between calculated data using the regression equation and those obtained experimentally.

The analysis of response surfaces

The relationship between the independent variables (X1 = S/L ratio, X2 = ultrasound amplitude and X3 = extraction time) and the dependent one (extraction efficiency, Y) was illustrated by three-dimensional plots of response surfaces (3D). Response surfaces provide a

way of visualizing the relationship between response and experimental levels of each variable, as well as the type of interaction between the variables.

The relationship between S/L ratios, ultrasound amplitude, extraction time and extraction efficiency is shown in ***Figures 4.7, 4.8*** and ***4.9.***

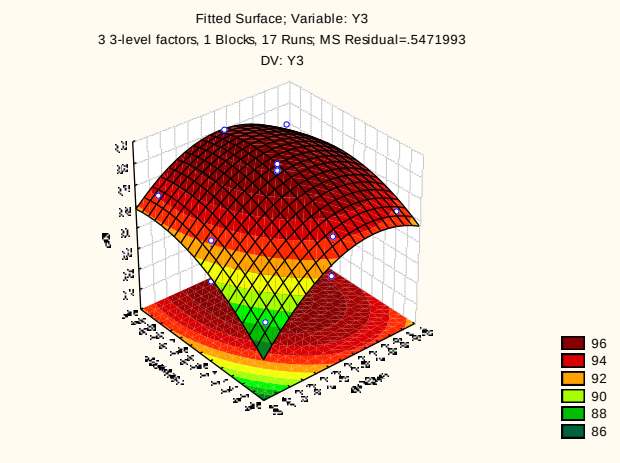

Figure 4.7. Response surface plots – influence of S/L ratio and amplitude on UAE oil extraction yield

Figure 4.7. shows the 3D surface graph and the contour graph of the effect of the S/L ratio (X1) and the amplitude (X2) on the extraction efficiency, while the extraction time (X3) is kept constant at zero (10 min). From ***Figure 4.7.*** it can be observed that the extraction yield increases with the amplitude (X2), reaches a maximum value in the middle of the value scale of S/L ratio, after which it decreases. The maximum extraction efficiency value (Y = 96%) is observed at 0.2 coded value (1/16.8 g/mL) for the S/L ratio (X1) and at about 1 (40%) for amplitude (X2).

Figure 4.8. shows the 3D surface graph and contour graph of the effect of the S/L ratio (X1) and extraction time (X3) on the extraction yield, while the amplitude (X2) is kept constant at zero coded value (30%). Oil extraction efficiency increases with the extraction time (X3) and reaches a maximum at the mid value of the S/L ratio (X1) scale. Thus, the maximum extraction efficiency point (Y = 96%) is observed at 0.2 coded value (1/16.8 g/mL) for the S/L ratio (X1) and somewhere close to 1 (between 0.8 and 1 ≈ 13 min) extraction time (X3).

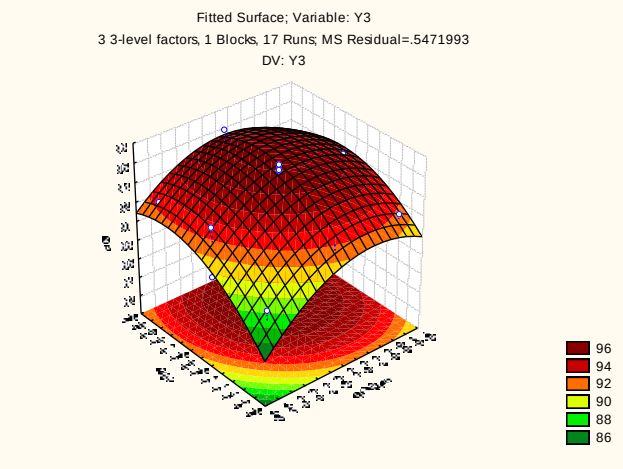

Figure 4.8. Response surface plots – influence of S/L ratio and extraction time on UAE oil extraction yield

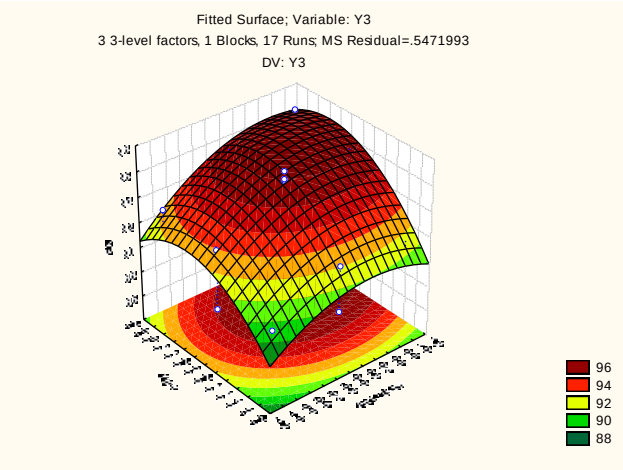

Figure 4.9. Response surface plots – influence of amplitude and extraction time on UAE oil extraction yield

Similar hypotheses are also valid for ***Figure 4.9.***, which shows the effect on extraction efficiency of amplitude (X2) and extraction time (X3), while the S/L ratio (X1) is kept constant at zero (1/16 g/mL). This time, extraction efficiency increases simultaneously with the ultrasound amplitude (X2) and extraction time (X3). The maximum extraction yield point (Y = 96%) corresponds to the maximum values of the two independent values, i.e. close to 1 (40%) for amplitude (X2) and close to 1 (15 min) for extraction time (X3).

The optimal working parameters, as determined using STATISTICA 10 software were: S/L ratio (X1=0), 1/16 g/mL; amplitude (X2=1), 40% and extraction time (X3=0.5), 12.5 min. The experimental value of the oil extraction efficiency (Y response) determined using the optimum extraction parameters was 96.88 ± 0.5%. This value is in good agreement with the predicted value of 97.02%.

4.3. TREATMENT OF THE OIL

We describe here a simple, laboratory-scale procedure for the treatment of crude *Lallemantia iberica* oil, using activated adsorbents, with the aim of making it suitable for a non-edible application, namely functionalisation and subsequent production of thermosetting resins.

4.3.1. Objectives of the oil treatment study

The treatment aimed at improving certain characteristics of crude LALO, in order to make it suitable for epoxidation or other functionalizations. The main characteristics were acidity, colour and iodine index.

4.3.2. Laboratory scale oil treatment

We analyzed comparatively a) two types of adsorbents, b) two different ratios oil:adsorbent, and c) cold and warm adsorbent treatments. Five experiments where conducted, each one in duplicate, varying the amount of adsorbent (10% and 20% wt of oil). The adsorbents used were: Engelhard grade F-160 (experiments 1 and 2) and alumina (experiments 3, 4 and 5). The alumina was milled before use.

The first and the third experiment consisted in treatment of the LALO with untreated E-F160 (first) and untreated alumina (for the third). In the experiments two and four, the oil treatment was carried out with cold calcined adsorbent, exp. 2 with E-F160 and exp. 4 with alumina; the adsorbent was previously calcined at 200-210°C for 30 min and then cooled. In the last experiment (exp. 5) the alumina was activated with 5% sodium hydroxide solution, calcinated at 200-210°C for 30 min and then allowed to cool to room temperature.

Results of oil treatment

The acid values data summarized in ***Table 4.15.*** show that the treatment with NaOH activated alumina leads to superior results, with reduction in acidity of about 96%. In the clay treatment, superior values are obtained if the adsorbent is previously dried.

Tabelul 4.15. Treatment results

Exp.	*Acronym*	*Treatment*	*Adsorbent proportion (wt % of oil)*	*Acid value (mg KOH)/g oil)*	*Free fatty acid (%)*	*Iodine value (g I/100g oil)*	*Max. UV absorbance (301 nm)*	*Bleaching capacity (%)*
E0	***LALO***	Crude LALO	-	5.24	2.64	193.84	2.401	
E1	***AER-2***	Untreated Engelhard F160	20%	4.63	2.33	198.70	0.752	68.68
	AER-1		10%	5.22	2.63	197.12	0.731	69.55

E2	***AEC-2***	Calcined Engelhard F160	20%	4.47	2.25	198.01	0.785	67.31
	AEC-1		10%	5.08	2.56	190.93	0.867	63.89
E3	***OAR-2***	Untreated alumina	20%	2.41	1.21	194.58	0.948	60.52
	OAR-1		10%	3.14	1.58	189.58	0.963	59.89
E4	***OAC-2***	Calcined alumina	20%	0.84	0.42	196.03	1.207	49.73
	OAC-1		10%	3.50	1.76	188.94	1.341	44.15
E5	***OAA-2***	NaOH activated & dried alumina	20%	0.39	0.2	191.62	1.344	44.02
	OAA-1		10%	2.04	1.03	189.91	1.162	51.60

It is important to note that iodine values, which were key to the outstanding properties of LALO, were not significantly affected by the adsorption treatment[47].

The amount of pigment removed was evaluated by calculating the bleaching capacity of the adsorbent [46, 51], as determined with the following equation (4.5):

$$\textbf{\textit{Bleaching capacity}} = 100*(A_0 - A)/A_0, \qquad (4.5)$$

where A_0 is the absorbance of the crude oil and A is the absorbance of treated oil.

The absorbance was measured using a diluted solution of *Lallemantia* oil in n-hexane (1:4, oil:hexane), at the maximum absorption wavelength (302 nm).

Table 4.15. and ***Figure 4.12.*** summarizes values from the UV-vis spectrum: the absorbance of the samples of LALO before and after treatments. ***Figure 4.12.*** shows the drop of absorbance values (the UV-Vis spectra of the treated samples) for the treated samples as compared to the untreated LALO spectrum.

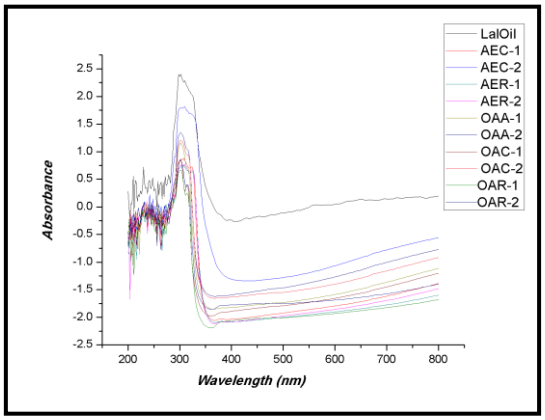

Figure 4.12. UV-vis spectrum of treated and crude LALO samples; solvent used: n-hexane

The data show that the most effective color reduction is obtained with Engelhard F-160.

4.4. CRUDE OIL CHARACTERIZATION

Crude *Lallemantia* oil was characterized by GC-MS, NMR, UV-Vis, in addition to basic lipid indices: acidity, iodine and saponification index.

As shown in ***Table 4.17.*** the main component of LALO is the highly unsaturated linolenic acid (64%), which determines the remarkable properties of the oil.

Table 4.17. Fatty acids profile of Lallemantia iberica oil

Lallemantia iberica oil (LALO)			
Peak	***Fatty Acid***	***Number of C atoms and double bonds***	***Mean***
1	Palmitic	C16-0	**6.635**
2	Palmitoleic (9 cis Hexadecenoic)	C16-1	**0.173**
3	Stearic	C18-0	**1.714**
4	cis-9-Oleic	C18-1	**13.313**
5	Linoleic	C18-2	**12.980**
6	cis-11-Eicosanoic	C20-1	**0.641**
7	Linolenic	C18-3	**64.367**
8	cis-11,14,17-Eicosatrienoic	C20-3	**0.177**

Figure 4.13. shows the ^{1}H-NMR spectrum of LALO, with signal assignments and chemical shifts listed in ***Table 4.18.***

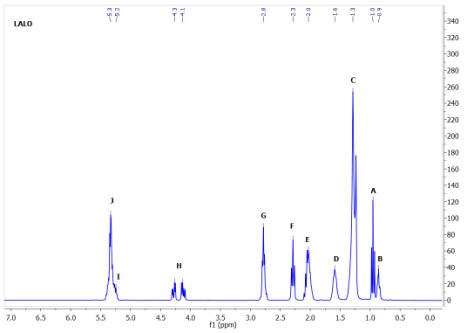

Figure 4.13. ^{1}H-NMR spectrum of Lallemantia iberica oil (LALO)

Table 4.18. Signal assignments and chemical schifts in ^{1}H- NMR spectrum of LALO

Signal	***δ (ppm)***	***Integral***	***Proton***	***Compound***
A	**0.95**	**4.97**	-CH=CH-CH2-C***H***3	Linolenic acid
B	**0.85**	**3.00**	-CH2-CH2-CH2-C***H***3	All alkyl chains, except for linolenic
C	**1.20**	**31.63**	-(C***H***2)$_n$-	All alkyl chains
D	**1.60**	**5.32**	-C***H***2-CH2-COOH	All alkyl chains
E	**2.02**	**9.36**	-C***H***2-CH=CH-	Allylic protons (all unsaturated fatty acids)
F	**2.20**	**5.22**	-C***H***2-COOH	All acyl chains
G	**2.76**	**7.11**	-CH=CH-C***H***2-CH=CH-	*Bis*-allylic protons (linoleic and linolenic acids)

H	**4.19**	**3.31**	-C***H***2OCOR	Glycerol (α position)
I	**5.15**		-C***H***OCOR	Glycerol (β position)
J	**5.29**	**12.72**	-C***H***=C***H***-	All unsaturated fatty acids

In the literature, the iodine index for *Lallemantia iberica* oil appears in the range of 185 to 205. The sample used in our study has a value of around 200. ***Table 4.19.*** presents the results obtained by three different methods.

Table 4.19. Iodine values of LALO determined with 3 methods

	Determination method for iodine index	***Iodine values ($gI_2/100g$)***	***Mean value***	***STDEV=SD (Standard deviation)***
1	GC chemometric determination	203,22		
2	NMR chemometric determination	199,13		
3	Titration – AOAC Hanus Method	193,84		
		596,19	***198,73***	***4,7028***

The standard deviation is less than 5% (4.7%), which shows satisfactory consistancy for this typical drying oil. The saponification value found for LALO was 196 mg KOH/g oil. This was also calculated chemometrically based on ^{1}H-NMR data [39]. The acid value (AV), as determined by titration according to the AOAC method [44], was 5.24 mg KOH / g oil. The free fatty acid (FFA) content of the oil can thus be calculated as 2.64%.

CAPITOLUL V. Synthesis of new polymer composites based on epoxidized vegetable oil and lignin

5.1. PRELIMINARY STUDIES FOR CHOOSING THE ADEQUATE COMPOSITIONS AND EXPERIMENTAL PROCEDURES

The present study aims to obtain compounds based on epoxidized vegetable oils (EVO) and their use in the preparation of composite materials using either unmodified or functionalized kraft lignin (LnK) as reinforcement. Specific steps are undertaken to identify cross-linking systems, suitable reaction conditions, varying also lignin proportions.

The experiments were carried out using two drying oils, namely *Lallemantia iberica* oil (LALO) and linseed oil (LO), with similar chemical characteristics (fatty acid profile, unsaturation index), *Lallemantia* oil being however superior in reactivity.

5.1.1. Preparation of composite materials

To obtain the EVO-LnK materials, several crosslinking systems currently used for epoxy resins were tried.

Protocol 1. Crosslinking with diamines.

The diamines used were 4,4'-diaminodiphenylmethane (DDM) and 1,6-hexamethylenediamine (HDA).

The proportions of diamine crosslinker were 27.5, 20 and 10% wt to EVO, and the reaction conditions 2h at 130 °C, followed by a post-crosslinking step for 1h at 150 ° C.

Protocol 2. Crosslinking with phthalic anhydride (PA) and 1-methyl-imidazole (1-MeI) catalyst.

The molar ratio EVO epoxy groups : PA was 1:1 with catalyst proportion 2% 1-MeI (relative to ELALO), using the reaction conditions indicated in Protocol 1.

Protocol 3. Crosslinking with a conventional Araldite class system.

The commercial Araldite system used was dodecenyl succinic anhydride (DDSA, HY964) as hardener and 2,4,6-tris-dimethylamino phenol (DY064) as accelerator.

The mass ratio of EVO:HY964 was 1:1 with a proportion of 10% accelerator DY064 (wt to ELO); the temperature used was 80 ºC and the time 23 hours.

Protocol 4. Crosslinking with UV radiation.

An attractive idea was to use photochemical cross-linking processes with the advantage of lower energy consumption and shorter reaction time. Triarylsulfonium hexafluoroantimonate (TSHA) was used as crosslinking photoinitiator.

The proportion of TSHA was 4% (wt to ELO); the amount was measured using a micropipette taking into account the density ρ 1.41 g/mL at 25 °C. The UV radiation used had a wavelength of 365 nm (Multiple-Ray Lamp – ***Figure 5.1.***), and the exposure time was 15 min.

Figure 5.1. UV Lamp – Analytik-jena (Multiple-Ray Lamp)

5.1.2. Results of preliminary studies

In this first study, we aimed to choose a crosslinking system that would allow a satisfactory homogenization of the oil-lignin mixture, leading to materials with a uniform composition, under acceptable reaction conditions (time, temperature). The first evaluation of the obtained materials was qualitative and visual (flexibility, hardness, polymerization time, uniformity of the material), followed by more complex characterizations (TGA, DMA, corrosion tests, etc.).

A summary of the preliminary experiments is presented in ***Table 5.2.***

Table 5.2. Summary of preliminary studies

Sample Code	***EVO & Crosslinking agent (proportion*)*** ***& Surfactant (proportion*)***	***Lignin*** ***(LnK/ELnK & proportion*)***	***Preparation & Crosslinking Conditions***	***Materials***
Protocol 1 – Diamines: DDM, HDA				
P1.1	***ELALO-DDM (27,5%)***	***Without LnK (reference sample)***	Thermal crosslinking – 2h at 130 °C, followed by a post-crosslinking step 1h at 150 °C.	*Unsatisfactory material.*
P1.2	***ELALO-HDA (27,5%)***	***Without LnK (reference sample)***	Thermal crosslinking – 2h at 130 °C, followed by a post-crosslinking step 1h at 150 °C.	*Uniform, relative flexible materials.*
P1.3	***ELALO-HDA (10%)***	***Without LnK (reference sample)***	Thermal crosslinking – 2h at 130 °C, followed by a post-crosslinking step 1h at 150 °C.	*Sticky material.*
P1.4	***ELALO-HDA (10%)***	***0,1% LnK***	Idem reference sample.	*Sticky material.*

P1.5	***ELALO-HDA (10%)***	***0,5% LnK***	Idem reference sample.	*Sticky material.*
P1.6	***ELALO-HDA (10%)***	***1% LnK***	Idem reference sample.	*Flexible material with poor tensile strength.*
P1.7	***ELALO-HDA (10%)***	***0,1% ELnK***	Idem reference sample.	*Flexible material with poor tensile strength.*
P1.8	***ELALO-HDA (10%)***	***0,5% ELnK***	Idem reference sample.	*Flexible material with poor tensile strength.*
P1.9	***ELALO-HDA (10%)***	***1% ELnK***	Idem reference sample.	*Flexible material with poor tensile strength.*
P1.10	***ELALO-HDA (20%)***	***5% LnK***	For efficient homogenization, the ELALO–LnK mixtures (5, 10, 20%) were subjected to an ultrasonic probe treatment for 5 min (amplitude 20%). Thermal crosslinking – 3h at 150 °C.	*Improved results: elastic materials, no longer sticky. However, the samples show an uneven dispersion; it appears that the lignin reacts to some extent with the diamine.*
P1.11	***ELALO-HDA (20%)***	***10% LnK***		
P1.12	***ELALO-HDA (20%)***	***20% LnK***		
P1.13	***ELALO-HDA (20%)***	***10% ELnK***	The ELALO–ELnK mixture (10%) was placed for 3 min in a sonication bath. Thermal crosslinking – 3h at 150 °C.	*The material is no longer sticky. The sample shows uneven dispersion.*
Protocol 2 – Phthalic anhydride (PA) + catalyst 1-methyl-imidazol (1-MeI)				
P2.1	***ELALO:PA (1:1), 1-MeI (2%)***	***Without LnK (reference sample)***	Thermal crosslinking – 2h at 130 °C, followed by a post-crosslinking step 1h at 150 °C.	*Unsatisfactory material.*
Protocol 3 – Araldite: hardener DDSA (HY964) + accelerator 2,4,6-tris-dimethylamino phenol (DY064)				
P3.1	***ELO:HY (1:1), without DY***	***Without LnK (reference sample)***	Thermal crosslinking – 6h at 130°C.	*Unsatisfactory material.*
P3.2	***ELO:HY (1:1), DY (10%)***	***Without LnK (reference sample)***	Thermal crosslinking – 23h at 80°C.	*Hard materials; transparent yellow color.*
P3.3	***ELO:HY (1:1), DY (10%)***	***20% LnK***	Thermal crosslinking – 23h at 80°C.	*Hard materials with low flexibility due to the reinforcing effect of lignin; opaque black color.*
P3.4	***ELO:HY (1:1), DY (10%)***	***35% LnK***	Thermal crosslinking – 23h at 80°C.	
P3.5	***ELO:HY (1:1), DY (10%)***	***50% LnK***	Thermal crosslinking – 23h at 80°C.	

P3.6	***ELO:HY (1:1), DY (10%)***	***20% ELnK***	Thermal crosslinking – 23h at 80°C.	*Hard materials with low flexibility due to the reinforcing effect imprinted by lignin; reddish-semi-transparent color.*
At Protocol 3 – attempts to improve LnK dispersion				
P3.7	***ELO:HY (1:1), DY (10%)***	***10% LnK***	***Method 1*** – manual homogenization & pre-crosslinking; mixing after the start of crosslinking at intervals of 1h, 2h and 3h respectively; then continued thermal crosslinking (total 23h at 80°C).	*Hard materials with low flexibility due to the reinforcing effect of lignin; opaque black color.*
P3.8	***ELO:HY (1:1), DY (10%)***	***20% LnK***	***Method 2*** – homogenization with ultrasonic probe & pre-crosslinking; the samples were kept under magnetic stirring, in an oil bath at 80 ºC; after 1, 2 and 3 hours of pre-crosslinking respectively, portions of the mixture were placed in teflon molds and continued thermal crosslinking (total 23h at 80°C).	*Hard materials with low flexibility due to the reinforcing effect of lignin; opaque black color.*
P3.9	***ELO:HY (1:1), DY (10%) & CTAB (1%)***	***10% LnK***	ELO-10%LnK-CTAB – manually mixed and subjected to treatment with an ultrasonic probe (20% amplitude) for 5 min. Thermal crosslinking – 23h at 80°C.	*Hard materials with low flexibility due to the reinforcing effect of lignin; opaque black color.*
P3.10	***ELO:HY (1:1), DY (10%) & DBS (1%)***	***10% LnK***	ELO-10%LnK-DBS – manually mixed and subjected to treatment with an ultrasonic probe (20% amplitude) for 5 min. Thermal crosslinking – 23h at 80°C.	*Hard materials with low flexibility due to the reinforcing effect of lignin; opaque black color.*
Protocol 4 – TSHA – UV				
P4.1	***ELO-TSHA (4%)***	***Without LnK (reference sample)***	UV Crosslinking, 15 min.	*Transparent materials, more flexible than those with Araldite.*
P4.2	***ELO-TSHA (4%)***	***5% LnK***	UV Crosslinking, 15-45 min.	*Unsatisfactory materials; they did not harden in depth, but formed a thin film on the surface of the material.*

****- Crosslinking agent/ lignin proportion is calculated with respect to oil quantity (ELALO/ELO).***

5.2. COATINGS BASED ON EPOXIDIZED LINSEED OIL AND KRAFT LIGNIN

5.2.1. Objectives of the study aimed at anticorrosive ELO-LnK coatings

We examined here the possibility of using non-functionalized lignin as component of a corrosion protection polymer. As a matrix for lignin, we used an ELO-based (epoxidized linseed oil – based) resin obtained by double cross-linking and chose LnK (kraft lignin) supplied by Sigma Aldrich, a complete characterization of the latter being recently reported [181]. The ELO-LnK composites were investigated by FTIR, TGA, DMA, CA, WAD and SEM. After synthesizing the resin, they were applied as coatings on carbon steel plates and evaluated for anti-corrosion performance.

5.2.2. Experimental protocol for obtaining anticorrosive ELO-LnK coatings

Several samples were prepared with ELO, HY964 and variables amounts of LnK (5% – sample S1, 10% – sample S2 and 15% – sample S3, respectively, calculated based on the amount of ELO). A reference sample (Sr) without LnK was formulated using the same procedure. All these can be found in ***Table 5.3.***. The samples coated with ELO-LnK (S1-S3 and Sr) were tested for anti-corrosion performance (***Figure 5.10.***). The remaining ELO-HY-DY-TSHA-LnK blends were cast into a silicone mold (20x35x2mm) and subjected to the same double crosslinking process. The obtained materials were characterized by various techniques.

Table 5.3. Samples prepared with ELO-HY-DY-TSHA-LnK

Sample Code	***Proportion of LnK relative to ELO***
Sr	Reference sample (without LnK)
S1	Sample with 5% LnK
S2	Sample with 10% LnK
S3	Sample with 15% LnK

Figure 5.10. Carbon steel plates coated with ELO-LnK based composite

5.2.3. Results of the study to obtain anticorrosive ELO-LnK coatings

ELO Characterization

The epoxidation of LO was monitored by means of ^{1}H-RMN and FTIR. Structural changes identified in the ^{1}H-NMR spectrum of ELO as compared to that of the crude oil confirm the epoxidation results.

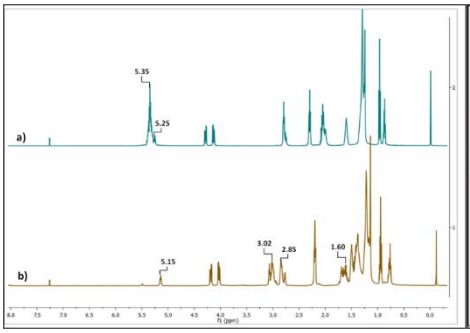

Figure 5.11. ^{1}H-NMR spectrum a) unmodified LO; b) epoxidized LO

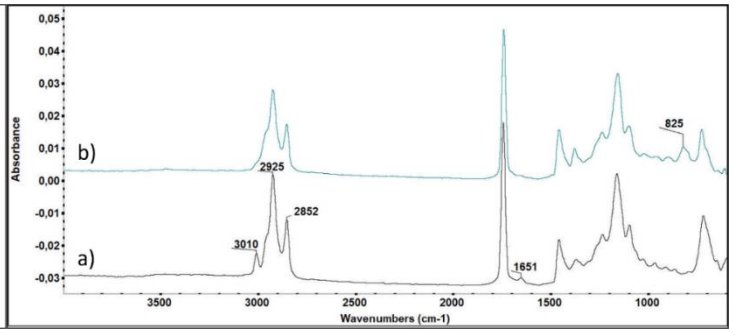

Figure 5.12. FTIR spectrum a) unmodified LO; b) epoxidized LO

FTIR analysis (***Figure 5.12.***) confirms the epoxidized structure of the monomer, through the appearance of the C–O–C stretching vibration band (epoxy rings) at 825 cm^{-1}.

ELO-LnK Composites Synthesis and Characterization

The ELO-LnK composites were investigated by Fourier transform infrared spectrometry (FTIR), thermogravimetric analysis (TGA), dynamic mechanical analysis (DMA), contact angle measurements (CA), water absorption degree (WAD) and scanning electron microscopy (SEM).

FTIR Spectrometry

The efficiency of the curing procedures used was assessed by FTIR spectrometry, in the 600-4000 cm^{-1} wave number region, before and after the dual treatment.

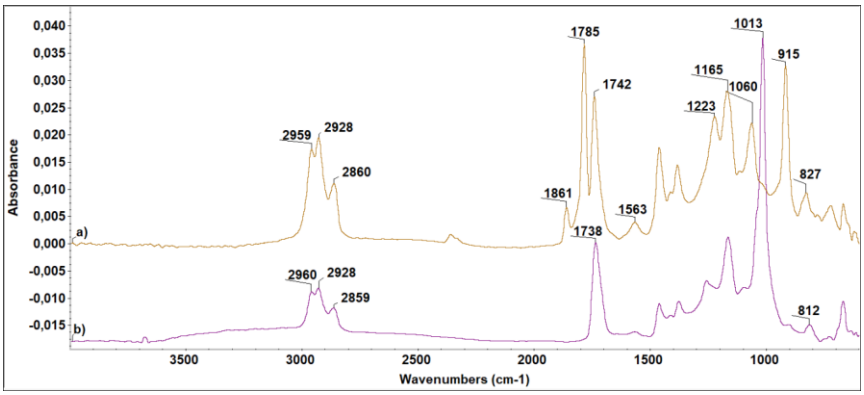

Figure 5.14. FTIR spectra of the S1 system (ELO+5%LnK) a) before and b) after dual-curing

In the b) spectrum of the cross-linked material ELO_LnK (***Figure 5.14.b***), the disappearance of the bands at 1785 and 1861 cm^{-1} of the carbonyl anhydride group is

observed. The appearance of the high intensity band at 1013 cm^{-1} is due to the new C-O bonds formed during the curing processes.

Additionally, GF measurements indicate a small unreacted fraction (maximum 8%) after the dual-treatment (UV and thermal curing). A slightly increase (3%) of the GF value was noticed for the S3 system compared to the reference sample (***Table 5.4.***).

Table 5.4. DMA, GF and contact angle results for ELO-LnK composites

Sample Code	**Tg[c] (ºC)**	**GF[d] (%)**	**θ[e] (°)**
Sr	55	92.06±0.54	84.82±1.72
S1	58	93.13±0.24	77.89±4.07
S2	62	93.95±0.22	73.97±1.46
S3	75	94.99±0.30	71.38±1.95

[c] – Tg = glass transition temperature considered as the maximum of tan δ plots

[d] – GF = gel fraction (the average of three measurements and corresponding standard deviation)

[e] – θ = water contact angle (the average of three measurements and corresponding standard deviation)

Thermo-gravimetric Analysis (TGA)

The thermal stability of the composites obtained by dual-curing treatment was investigated by TGA, in N_2 atmosphere as well as in presence of air. Results are summarized in ***Table 5.5.***

Table 5.5. TGA data of ELO-LnK materials (N_2 and air)

N_2								
Sample Code	***Weight Loss***				***Degradation Steps (ºC)***			***Weight Change at 700ºC (%)***
	T_d[a]				**T_{max}[b]**			
	3% (ºC)	**10% (ºC)**	**30% (ºC)**	**50% (ºC)**	**1 (ºC)**	**2 (ºC)**	**3 (ºC)**	
Sr	185	223	320	358	234	365	448s	99
S1	197	247	339	366	243	365	440s	96
S2	192	242	336	364	230	362	448s	91
S3	197	256	343	370	250	363	449s	88
LnK	159	258	355	502	-	353	-	61
Air								
Sample Code	***Weight Loss***				***Degradation Steps (ºC)***			
	T_d[a]				**T_{max}[b]**			

	3% (ºC)	**10%** (ºC)	**30%** (ºC)	**50%** (ºC)	**1** (ºC)	**2** (ºC)	**3** (ºC)	**4** (ºC)	***Weight Change at 700ºC (%)***
Sr	193	242	336	383	230	333	375 421s	527	88
S1	199	256	346	387	260	339	378 426s	520	85
S2	191	243	332	374	243	338	376 417s	509	98
S3	182	229	325	373	224	336	376 395 429s	503	98
LnK	86	255	395	436	-	-	448	-	93

[a] – T_d = the thermal degradation temperature as the weight loss of material at 3, 10, 30, 50%

[b] – T_{max} = temperature at which the maximum mass decomposition occurs

[s] – shoulder

When LnK is loaded, a lower degradation rate was noticed for all samples (S1-S3) as compared to the reference sample Sr, indicating an improved thermal stability associated with the aromatic structure of the lignin.

As can be seen from the weight loss curves (***Figure 5.15.a***), above 300°C the reference material (Sr) decomposes faster leading to lower residual char at 700 °C (1%), due to the complete decomposition of the LO aliphatic chains. The increase of residual mass at 700°C for the S1-S3 composites could be explained by the crosslinked phenolic-type structure of LnK, which does not easily break down [224].

All DTG curves showed a three-step decomposition behaviour (***Figure 5.15.b***). The last weight loss (of ~15%), is reflected in the DTG curves as a shoulder around 450°C, which probably corresponds to C-C bond cleavage [225].

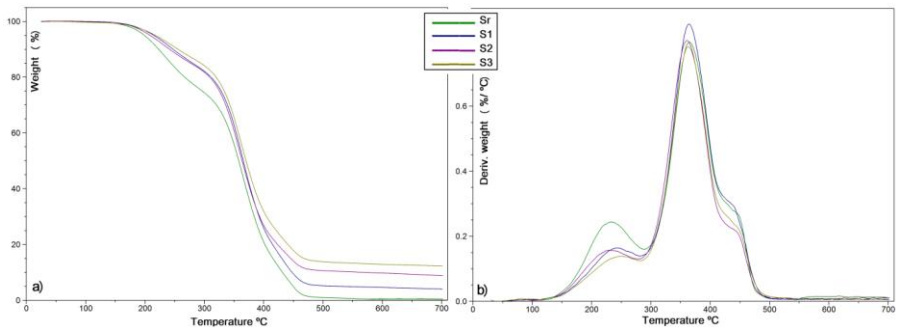

Figure 5.15. a) TGA and b) DTG curves for ELO-derived composite materials (N_2)

In presence of air ELO-LnK composites show a more complex decomposition behaviour (***Table 5.5.***). Curve shapes are slightly dependent on the LnK proportion in the composite (***Figure 5.16.a,b***), the decomposition process under thermo-oxidative condition being faster once the proportion of the LnK increases. The system with lower LnK percentage (S1, 5% wt. LnK) seems to be the more thermo-stable material in oxidative environment.

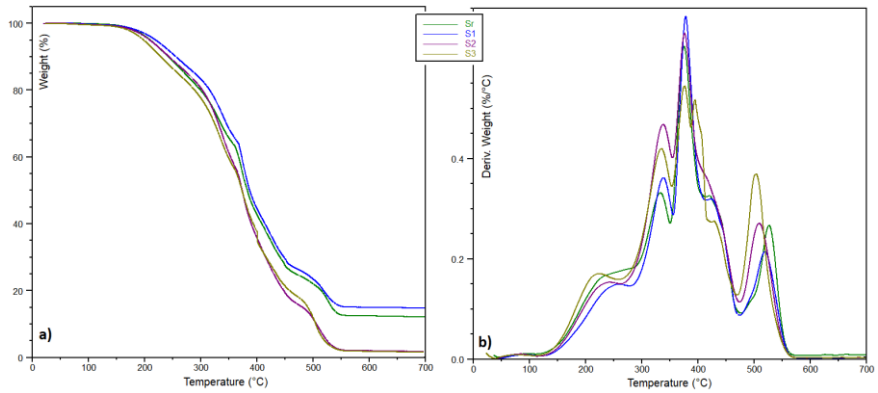

Figure 5.16. Thermal degradation profile (air) of ELO-LnK materials.
a) TGA and b) DTG curves

Morphology Investigation (SEM)

Figure 5.18. shows SEM photographs of the fractured samples Sr, S1, S2 and S3, at 5000X magnification. Certain architectural differences associated with the LnK content are noticed. The fracture surface of the neat epoxy polymer (***Figure 5.18.Sr***) is very smooth except for the regular button-shape, observed in the cross section, which comes from the incorporated THA photo-initiator. This attribution has been proved by SEM-EDX analysis (***Figure 5.19.***).

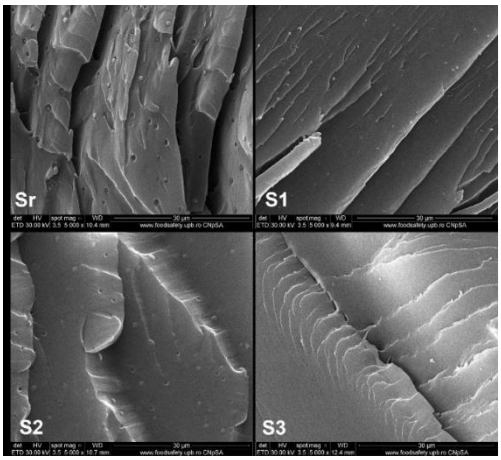

Figure 5.18. SEM images of ELO-LnK composites (5000X)
Sr: ELO polymer; S1: ELO+5%LnK; S2: ELO+10%LnK; S3: ELO+15%LnK

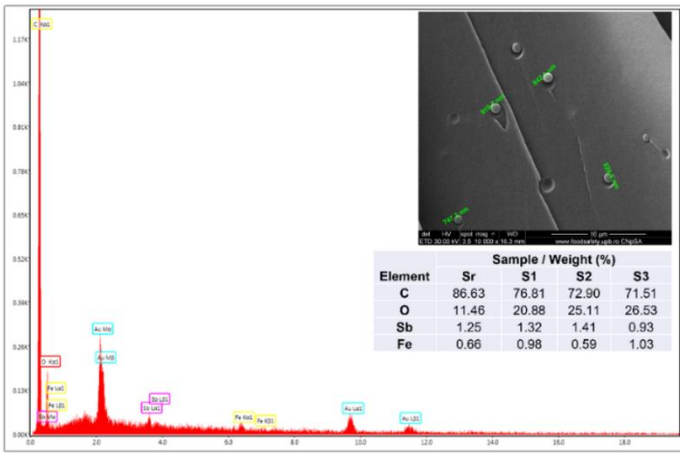

Figure 5.19. Qualitative SEM-EDX for Sr sample (SEM – 1000x magnification)
Insertion: quantitative results for Sr

Water Affinity (CA & WAD)

Static water contact angle measurements (CA) and water absorption experiments (WAD) were carried out in order to evaluate the wettability of the composites. The results are shown in ***Table 5.4.*** and ***Figure 5.20.***, respectively. Generally, water affinity has a direct effect on corrosion susceptibility, more hydrophobic surfaces conferring enhanced resistance against wet corrosion [201].

Lignin, which has both hydrophilic and hydrophobic units, may influence the wetting properties of the final materials in both directions. The sample with 15% wt. LnK concentration (S3) registered the lowest contact angle, around 71°, the differences between the neat Sr sample and S1 (containing 5% wt. LnK) being just 8°. If LnK-loaded composites are compared with the reference sample, the decrease of the CA values is not too high considering the large number of –OH groups (phenolic and aliphatic) of the LnK structure.

To elucidate the bulk water affinity of ELO-LnK composites, water absorption degree (WAD) was investigated during 10 days, using a ASTM D570 method. The WAD graph (***Figure 5.20.***) reveals a low water affinity after 10 days of immersion: 7.26% for S1, 8.83% for S2 and 12.42% for S3. These values are promising for the corrosion protection application when compared with other lignin-epoxy composites [227].

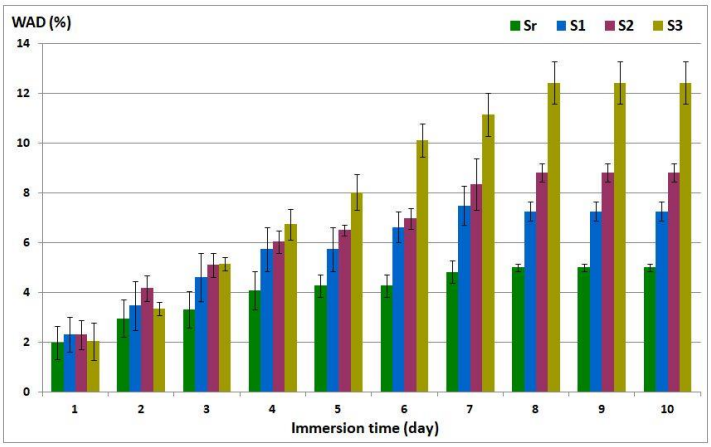

Figure 5.20. Water absorption degree for ELO-LnK composites

Electrochemical measurements

The anticorrosion performance of ELO-LnK composites was evaluated using coated carbon steel sheets. Potentiodynamic polarization experiments in 3.5% NaCl solution for 30 minutes (***Figure 5.22.***) were conducted, recording Tafel curves at a sweep rate of 2.5 mV/s, in the potential range from –0.8 V/ SSCS to +0.8 V/ SSCS. ***Table 5.6.*** presents corrosion

parameters such as corrosion potential (E_{corr}), corrosion current density (i_{corr}), polarization resistance (Rp) for the carbon steel sheets coated with ELO-LnK layers, together with cathodic (βc) and anodic (βa) Tafel slopes and inhibition efficiency (*IE*).

Table 5.6. Electrochemical parameters calculated from Tafel polarization curves

Sample Code	***E_{corr} (mV/SSCS)***	***i_{corr} (μA/cm²)***	***Rp (kohm*cm²)***	***βa (mV)***	***- βc (mV)***	***Correlation Coefficient***	***IE (%)***
*OL**	-646	1.5531	12.64	75.3	257.3	0.9999	-
Sr	-584	0.5562	52.71	180.8	185.0	0.9977	64.19
S1	-581	0.0015	19,930.00	186.1	188.3	0.9974	99.90
S2	-558	0.1036	282.20	185.1	183.3	0.9977	93.33
S3	-523	0.0601	450.26	171.0	170.6	0.9977	96.13

**OL – the uncoated carbon steel sheets (blank)*

The Tafel graphs (***Figure 5.22.***) show clearly that all ELO-based coatings exhibit a corrosion inhibition effect, significantly reducing the density of the corrosion current. With 5% LnK (S1 sample) the corrosion rate is reduced by up to 2 orders of magnitude compared with the uncoated sample (OL). The highest efficiency against corrosion, namely 99.9%, is exhibited by the S1 sample.

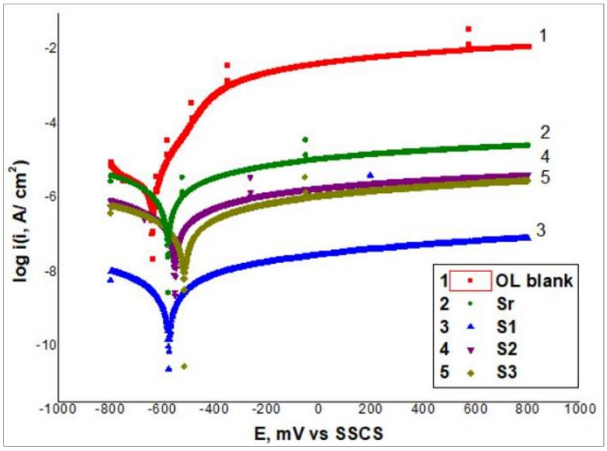

Figure 5.22. Potentiodynamic polarization (Tafel) curves for uncoated and coated samples in 3.5% NaCl solution at 25⁰C

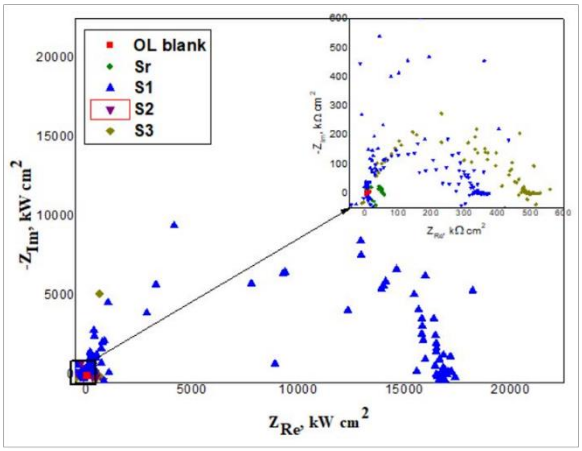

Figure 5.23. Nyquist plots after accelerated corrosion test in 3.5% NaCl solution at 25⁰C

OL – uncoated carbon steel sheet (blank)

Electrochemical impedance spectroscopy (EIS) measurements were performed on the coated steel samples. *Nyquist plots* were registered before the potentiodynamic polarization test in aggressive environment (*after 30 min immersion*) as well as after the test (*after accelerated corrosion test*) (***Figure 5.23.***). ***Table 5.7.*** shows the electrochemical parameters

such as electrolyte resistance (*R1*), coating resistance (*R2*), double layer capacitance (*Cdl*), as well as inhibition efficiency (IE).

Table 5.7. Electrochemical parameters obtained from EIS measurements, after 30 minutes immersion and after the accelerated corrosion test in the 3.5% NaCl solution at 25 ^{0}C

Sample Code	After 30 min immersion				After accelerated corrosion test			
	R1 (ohm*cm²)	R2 (kohm*cm²)	Cdl (pF/cm²)	IE (%)	R1 (ohm*cm²)	R2 (kohm*cm²)	Cdl (pF/cm²)	IE (%)
*OL**	111.80	6.48	43.69 10^6	-	45.83	37.50	84.87 10^6	-
Sr	63.83	41.43	307.30	84.35	38.52	49.53	321.20	24.29
S1	92.99	20,600.00	691.90	99.97	41.63	17,350.00	366.80	99.78
S2	132.00	405.90	43.90	98.40	224.00	596.30	53.37	93.71
S3	70.04	390.40	290.10	98.34	40.90	501.70	225.80	92.53

**OL – the uncoated carbon steel sheets (blank)*

As shown in ***Table 5.7.***, after the 30 min immersion required to stabilize the system in the aggressive environment, LnK-loaded coatings indicated a superior corrosion performance, S1 (5% LnK) being the more efficient. The results after accelerated corrosion test are found to be comparable with those obtained after 30 min immersion.

The Nyquist recorded spectra (***Figure 5.23.***), show a semicircle, the higher diameter being associated with the S1 sample (5% LnK). These results are in good agreement with those obtained from Tafel measurements.

5.3. COMPOSITES BASED ON EPOXIDIZED *LALLEMANTIA* OIL AND FUNCTIONALIZED LIGNIN

5.3.1. Objectives of the study to obtain ELALO-ELnK composites

In the present study, different types of composite materials based on ELALO (epoxidized *Lallemantia* oil) and ELnK (epoxidized kraft lignin) were obtained. For a better dispersion of the lignin particles, three additives as SDA (structure directing agents) were tested. The resulting ELALO-ELnK type composite materials were investigated by different characterization techniques, the physico-chemical, thermal, thermo-mechanical, morphological properties, affinity for water, as well as the relationship between structure and properties being established.

5.3.2. Experimental protocol for obtaining ELALO-ELnK composites

Three types of SDA were used in the formulation of ELALO-ELnK systems, with the aim of improving the dispersion of the reinforcing agent. Each SDA was added as 1% (wt)

based on the amount of ELALO. Two concentrations of ELnk were tested, 1% and 5% (wt, with respect to ELALO). ELALO-ELnK composites were synthesized using UV crosslinking in the presence of TSHA photoinitiator. A number of 12 samples (F1-F12) were prepared as shown in ***Table 5.8.***, including a reference sample (F1), without SDA and ELnK, following the experimental procedure described in ***Section 3.2.8***.

Table 5.8. Composition of ELALO-SDA-ELnK systems

Sample code	***Sample description***	***Additives***			
			SDA[b]		
		ELnK[a]	***DBS[c]***	***Span 60[d]***	***HSA[e]***
F1	ELALO	0	0	0	0
F2	ELALO-DBS	0	1%	0	0
F3	ELALO-Span	0	0	1%	0
F4	ELALO-HSA	0	0	0	1%
F5	ELALO-ELnK1%	1%	0	0	0
F6	ELALO-ELnK5%	5%	0	0	0
F7	ELALO-DBS-ELnK1%	1%	1%	0	0
F8	ELALO-Span-ELnK1%	1%	0	1%	0
F9	ELALO-HSA-ELnK1%	1%	0	0	1%
F10	ELALO-DBS-ELnK5%	5%	1%	0	0
F11	ELALO-Span-ELnK5%	5%	0	1%	0
F12	ELALO-HSA-ELnK5%	5%	0	0	1%

[a] – LnK functionalized with epoxy rings; [b] – structure directing agents; [c] – dibenzylidene sorbitol; [d] – sorbitane monostearate; [e] – 12-hydroxystearic acid.

5.3.3. Results of the study to obtain ELALO-ELnK composites

ELALO Characterization

The epoxidation of LALO was monitored using ^{1}H-NMR and FTIR. The ^{1}H-NMR (***Figure 5.24.a,b***) and FTIR (***Figure 5.25.a,b***) spectra, recorded for the ELALO derivative, as compared to LALO, confirmed the epoxidation reaction. The new ^{1}H-NMR signals (at 3.04 ppm, 2.86 ppm and 1.70 ppm) can be attributed to internal and marginal protons belonging to the epoxy rings, and to neighboring -CH2 groups located between two epoxy rings (for linoleic and linolenic acid moieties). In the FTIR spectrum the presence of epoxy rings is evidenced by the new absorption bands in the 815 – 960 cm^{-1} area. As expected, the ^{1}H-NMR double bond signal at 5.33 ppm disappeared (***Figure 5.24.a.***), as a result of the epoxidation, while in the ELALO FTIR spectrum (***Figure 5.25.b.***) the absorption bands at 3010 and 1654

cm^{-1} (ν_{Csp2-H} and $\nu_{C=C}$ respectively), previously seen in the LALO spectrum (***Figure 5.25.a.***), are now absent.

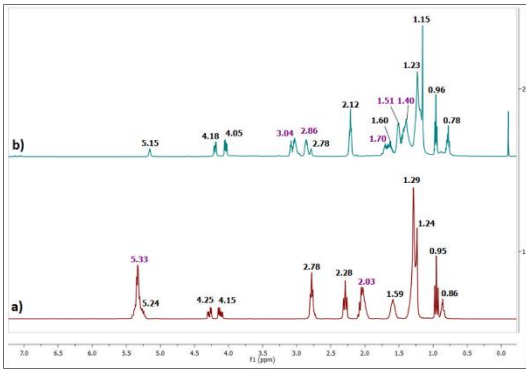

Figure 5.24. ^{1}H-NMR spectrum a) unmodified LALO; b) epoxidized LALO (ELALO)

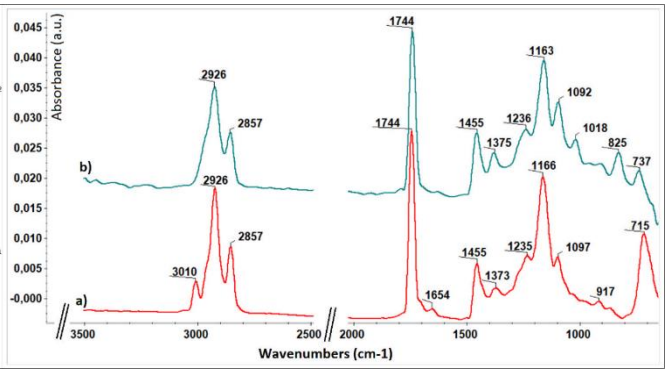

Figure 5.25. FTIR spectrum a) unmodified LALO; b) epoxidized LALO (ELALO)

Characterization of epoxidized lignin (ELnK)

The functionalization of LnK with epoxy rings was carried out according to a literature method [180], as described in ***Section 3.2.6.***. The FTIR spectrum recorded for ELnK (***Figure 5.26.b.***) shows new elements in the range 1300-1200 cm^{-1}, due to the presence of new C-O (ether) bonds [180]. The bands from 1701 – 1596 cm^{-1} can be attributed to epoxide groups and to ether bonds (C-O-C), with the participation of phenol and alcohol OH groups from the lignin structure [170].

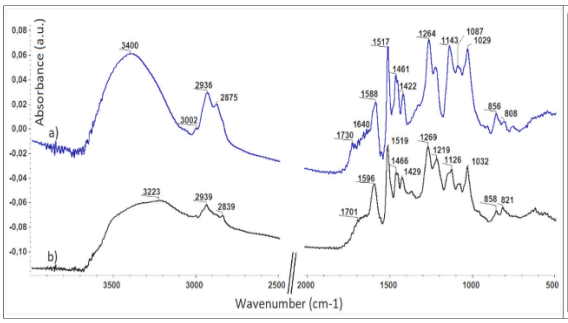

Figure 5.26. FTIR spectrum a) unmodified LnK; b) epoxidized LnK (ELnK)

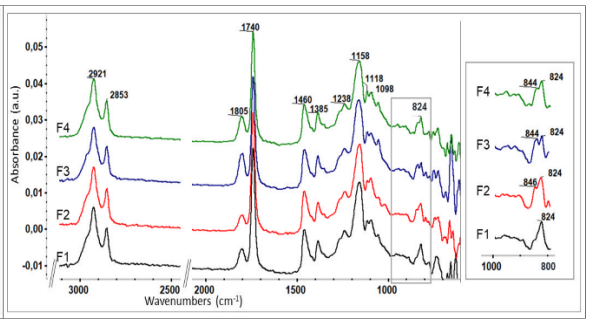

Figure 5.27. FTIR spectrum of F1-F4 unpolymerized systems. Detail-cropped & zoomed from 1000-800cm^{-1}

Synthesis and characterization of ELALO-ELnK composites

SDA effect on the ELALO structure

The influence of SDA addition on the structural arrangements of the formulations studied was investigated by means of FTIR spectroscopy. ***Figure 5.27.*** shows the spectra of the unpolymerized systems F1-F4. No major difference was observed when F2-F4 spectra were compared to the reference system F1.

In each F2-F4 case, it is possible for SDA molecules to form H bonds with ELALO monomer, organizing its structure, this type of bonds being the main interactions through

which DBS molecules can form fibrillar structures. The DBS-methyl methacrylate systems reported [231] indicated the formation of H bonds between DBS molecules and C=O ester bonds. For the ELALO-DBS formulations (F2), due to the high degree of functionalization (ELALO), the added DBS is expected to form H-bonds with the oxygen atoms of the oxirane moieties.

The SDA influence on the polymerization process

Figure 5.28. shows FTIR spectra recorded for ELALO-SDA materials (F1-F4) after cross-linking. New absorption bands are observed in the spectral region 1022-1077cm^{-1} attributed to different stretching and deformation vibrations of C-C-O, C-O and O-H bonds, formed during the photo-polymerization reaction. Also, O-H stretching vibration bands can be observed for all samples F1-F4, in the spectral region 3000-3500 cm^{-1}, as a result of ring opening.

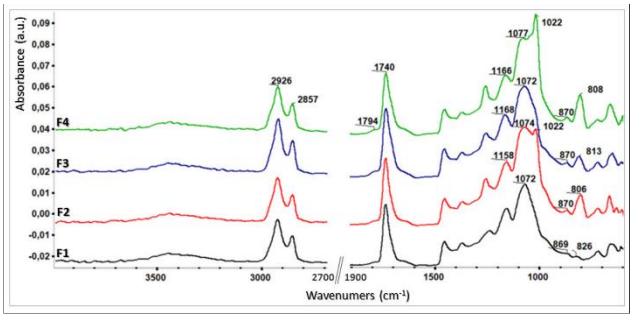

Figure 5.28. FTIR spectrum of F1-F4 UV crosslinked systems

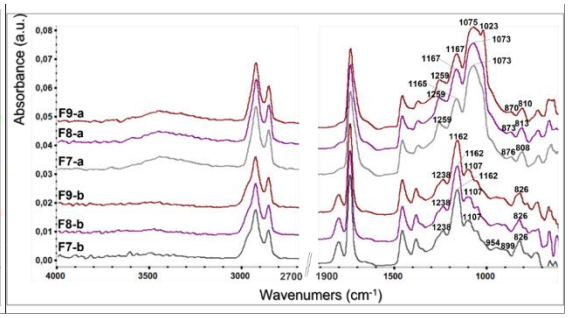

Figure 5.29. FTIR spectrum of ELALO-SDA (F7-F9) systems b-before UV a-after UV

In ***Figure 5.29.*** in case of cross-linked materials (spectra F7-a – F9-a) structural differences are observed for the different incorporated SDA. The spectra of F7-a and F8-a (DBS and Span 60) indicate the presence of an absorption maximum at 1073 cm^{-1}, while F9-a (HSA) indicates also a second maximum located at 1023 cm^{-1}. The changes in the area 3200-3500 cm^{-1}, appearing in the spectra of photo-polymerized systems (F7-a – F9-a), confirm the ring opening reaction and the formation of O-H bonds.

Conversion of the epoxy groups by GF measurements

The calculated GF values (***Table 5.9.***) indicate a slightly positive influence on the epoxy ring conversion under UV treatment. The highest GF values were obtained, according to ***Table 5.9.***, in the case of using Span and HSA, for the systems with 1% ELnK (F8 and F9). Unfortunately, for systems with 5% ELnK, GF measurements indicate a lower conversion of epoxy groups, due to the known UV stabilizing effect of lignin and its derivatives, which act as a radiation blocking agent [189,232].

Table 5.9. GF, CA, WAD and DMA results

Sample Code	*GF (%)*[a]	*CA (°)*[b]	*WAD (%)*[c]	*Tg (°C)*[d]
F1	97.06 ± 0.49	84.24 ± 2.48	1.27 ± 0.36	64
F2	95.14 ± 0.31	81.72 ± 2.79	1.73 ± 0.20	63
F3	97.32 ± 0.48	102.84 ± 1.06	0.60 ± 0.30	59
F4	96.04 ± 0.83	89.88 ± 1.14	2.11 ± 0.44	61
F5	95.91 ± 0,50	94.50 ± 0.96	2.03 ± 0.30	65
F6	79.41 ± 4,77	70.05 ± 1.58	*not determined*	*not determined*
F7	96.60 ± 0,56	84.02 ± 2.48	1.72 ± 0.67	56
F8	97.40 ± 0.46	94.28 ± 2.68	1.02 ± 0.19	60
F9	97.10 ± 0.20	82.56 ± 2.62	2.30 ± 0.19	59
F10	80.66 ± 0.51	88.08 ± 2.46	*not determined*	*not determined*
F11	84.18 ± 0.66	87.18 ± 2.00	*not determined*	*not determined*
F12	68.05 ± 1,86	82.40 ± 3.08	*not determined*	*not determined*

[a] – GF = gel fraction (the average of three measurements and corresponding standard deviation)

[b] – CA = water contact angle (the average of three measurements and corresponding standard deviation)

[c] – WAD = water absorbtion degree

[d] – Tg = glass transition temperature

Water affinity of ELALO-based materials

Surface and bulk wetting properties were investigated by contact angle (CA) and water absorption degree (WAD; WA, at 24 h) measurements (***Table 5.9.***). CA values are directly influenced by the chemical nature of SDA, Span 60 leading to materials with more hydrophobic surfaces compared to the reference sample (103° for F3 and 84° for F1, respectively), while DBS (F2) led to a more hydrophilic material. For samples containing ELnK (without SDA addition), 10° higher (F5) and 15° lower (F6) CA values were obtained for an additive concentration of 1% and 5%, respectively. This behavior is probably related to the structure of lignin which contains both hydrophilic and hydrophobic units.

The results obtained from the CA measurements are consistent with those calculated for the WAD study, with F3 and F8 being the most hydrophobic materials, both on the surface and in bulk, both containing SDA Span 60 as an additive.

Morphology investigation (SEM)

Figure 5.30. shows SEM images of systems F1 (control), F5 (ELALO-1%ELnK), F7-F9 (ELALO-1%ELnK with F7-DBS, F8-Span, F9-HSA), analyzed in fracture, at a

magnification of 2000X. For the reference sample (F1), the classic morphology of polymers derived from epoxidized oil is observed. This does not show major changes with the addition of ELnK (F5). In the case of the F7-F9 systems, it is observed how each type of SDA added leads to perceptible architectural changes. The addition of Span 60 (sample F8) leads to a uniform material, while HSA (sample F9) causes a coarse (rough) architecture, similar to the morphology of gels obtained from rapeseed oil with 2% HSA [233].

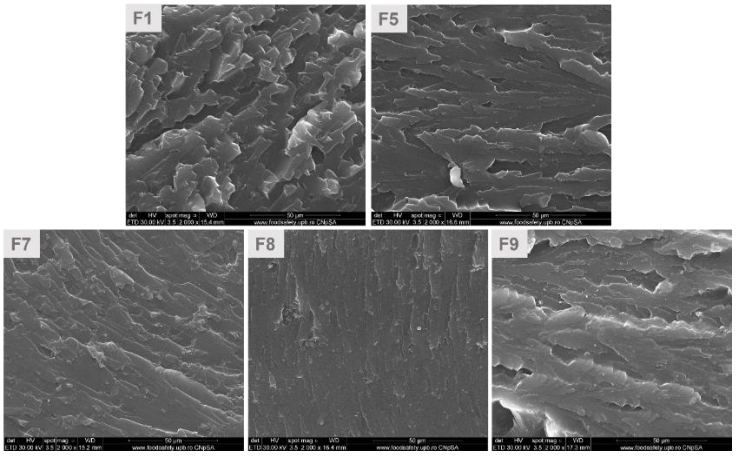

Figure 5.30. SEM images for ELALO-SDA samples (F1, F5, F7 – F9)

Thermo-mechanical analysis (DMA)

From the recorded DMA curves (***Figure 5.31.***) it can be seen that Span 60 (F3) and HSA (F4) slightly decrease the Tg values, due to the structures with long chains, which can induce flexibility. On the other hand, the addition of ELnK (F5) does not seem to have a significant effect on the thermo-mechanical characteristics of ELALO, probably because of the low concentration used (1%). When both types of additives (both SDA and lignin derivative) were used, the same slight influence was observed. These DMA results indicate that ELnK does not act as a reinforcement agent. The general behavior observed for the studied ELALO-SDA-ELnK materials, as well as the shape of the recorded thermograms, with a single maximum (associated Tg), is an indication that the developed materials are homogeneous.

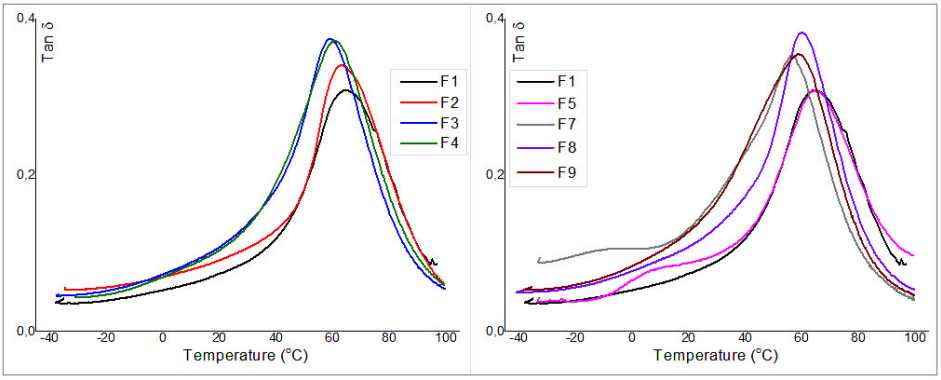

Figure 5.31. DMA curves (Tan δ vs. temperature) recorded for selected ELALO-based materials. SDA influence – left graph and influence of both additives (SDA & ELnK) – right graph

Thermo-gravimetric analysis (TGA)

The thermal stability of ELALO-based systems was not dramatically affected by the addition of different types of SDA in the early stages of the degradation study, with only Span 60 (F3) leading to a slight decrease in thermal properties in this first heating interval. As the experiment progresses, a noticeable decrease in the thermal stability of the ELALO-SDA materials was observed, Span 60 (F3) being the additive that stands out for this less favorable influence (the $Td_{10\%}$ value decreases by ~5%, compared to the reference sample – F1).

For samples loaded with ELnK, F5 and F6, an improved thermal degradation profile was observed over the entire temperature range of the experiment, explained by the presence of epoxidized lignin.

Table 5.10. TGA results (N_2 atmosphere)

Sample Code	***Weight loss – Td (°C)***				***Tmax (°C)***	***Residual mass (%, at 700°C)***
	3%	***5%***	***10%***	***50%***	***Tmax***	
F1	168	211	331	407	404	2.18
F2	168	211	324	407	404	2.63
F3	164	201	313	407	404	3.98
F4	167	208	319	407	404	2.46
F5	178	229	333	408	407	3.84
F6	179	235	337	409	414	5.53
F7	175	216	326	408	405	4.21
F8	172	245	335	409	408	4.50
F9	173	232	334	410	407	4.47
F10	176	240	332	408	406	6.25
F11	176	252	332	405	403	3.46
F12	179	250	336	409	404	7.36

The use of SDA in the synthesis of ELALO-ELnK composites improves the thermal stability, leading to homogeneous polymer composites. The system with Span 60 (F8) recorded the best thermal stability.

5. CONCLUSIONS

The following conclusions emerged from the studies presented in this paper:

1. ***Optimization of extraction, pre-treatment of the oil and its characterization.***

1.1. Following some preliminary experiments, ultrasound-assisted extraction (UAE) was chosen as the method of choice. Compared to conventional extraction methods, UAE is cheap, fast and therefore efficient. Soxhlet extraction, considered one of the methods that ensures a high yield, was chosen as a reference in the optimization process.

1.2. Extraction yield was used as dependent variable in the optimization equation. UAE parameters were optimized using a statistical method called response surface methodology (RSM).

1.3. The following factors, each with three levels, were chosen as independent variable parameters influencing the extraction yield (Y): solid/liquid ratio (X1), ultrasound amplitude (X2) and extraction time (X3). The effects of these three parameters on the extraction yield were investigated using a mathematical model, namely the Box-Bencken design. The polynomial equation obtained could be used to calculate the extraction yield.

1.4. Using the methods presented above in 1.1., 1.2. and 1.3., the optimal values of the extraction parameters were obtained and according to them the theoretical yield was calculated. These values were verified by comparison with experimentally obtained ones. The results of these comparisons showed a very good agreement between the calculated and the experimental yield. The experimental value obtained for the optimal conditions was ***96.88%***, which corresponds to an oil content of 39.67 g/100 g seeds. This value is in agreement with the predicted value of ***97.02%***, calculated using the model (corresponding to an oil content of 39.73 g/100 g seeds). The Box–Behnken model showed also that the two primary factors influencing the dependent variable were extraction time (the linear term) and the squared term of the S/L ratio.

1.5. *Lallemantia* oil was characterized using the following parameters: acid value, iodine value, saponification index and fatty acid profile. The methods used were: GC-MS, NMR, UV-Vis. The analysis of extracted LALO confirmed a high

content of linolenic acid (64%), which confers the oil a remarkable application potential as a drying oil.

1.6. The extracted oil was treated with two types of adsorbents: clay and aluminum oxide. The quality improvement of treated LALO depended on the nature of the adsorbent used, its pretreatment and the mode of operation. Thus, the E-F160 treatment provided better bleaching results, while the aluminum oxide treatment resulted in a more efficient reduction of oil acidity. Alumina activation with sodium hydroxide was found to increase the treatment efficiency, resulting in acid index values reduced to almost zero (0.39 – in the case of the 20% adsorbent treatment), the reduction in acidity, as expected, being more pronounced if a larger amount of activated alumina is used.

2. <u>Preparation of ELO-LnK and ELALO-ELnK composites. Applications.</u>

2.1. Epoxidized *Lallemantia* oil (ELALO) proved to be a suitable starting material for the synthesis of a polymer matrix.

2.2. The possibility of using lignin (LnK, ELnK) as a filler in a matrix based on ELALO and ELO was well confirmed. Lignin was chosen due to advantages such as: a) abundance in nature; b) its specific reactivity, for example due to free hydroxyl groups; c) remarkable stability; d) the possibility of being modified, for instance by hydrolysis or by functionalization.

2.3. Araldite was chosen as the crosslinking agent because the resulting material has superior properties, for both reference and lignin-containing samples.

2.4. Non-functionalized kraft lignin (LnK) proved to be an important element of the synthesized composites rendering them superior hardness and therefore designating them as a promising candidate for anti-corrosion application.

2.5. Compared to unmodified lignin (LnK), epoxidized lignin (ELnK) seems to lead to composite materials with even more interesting properties. Comparing the samples with Araldite, those with kraft lignin are opaque (black), which suggests a simple mechanical dispersion, with a reduced degree of chemical affinity between matrix and filler. The samples with epoxidized lignin are semi-transparent (reddish); the latter, although involving an additional step for functionalization, present a better incorporated filler. This was probably due to a chemical reaction between resin and lignin rests, leading to a continuity of

structure throughout the composite. A much stronger and more stable material is then to be expected.

2.6. The use of surfactants improved the experimental procedure, leading to materials with a more uniform composition.

2.7. In the case of UV crosslinking, more flexible reference samples (without LnK) than those with Araldite were obtained, the crosslinking time being only 10-15 min. This approach, beyond the obvious environmental advantages, is interesting both technically and economically. For the continuation of the studies we decided to keep using UV crosslinking, in order to benefit from the flexibility of the samples obtained. This property is important in the case of metal coating because it can prevent damage to the film when the support undergoes geometric changes or is subjected to mechanical stress.

ELO-LnK composites for anticorrosion coatings

2.8. Unfunctionalized kraft lignin (LnK) was incorporated in a corrosion protection polymer. Epoxidized linseed oil (ELO) resin was used as the lignin matrix. The latter was obtained by double cross-linking (UV radiation and thermal curing) in order to ensure a good lignin dispersion. The ELO-LnK composites were characterized by FTIR, TGA, DMA, CA, WAD and SEM.

2.9. The presence of LnK was found to improve the thermostability of composites. The thermal degradation behavior under inert gas (N2) indicated that the higher the LnK content, the better the thermal composite stability, while for the experiment in air, the material with the lower LnK content (5%) was the most thermostable.

2.10. ELO-LnK composites showed promising corrosion protection performances. They were tested as coatings for carbon steel sheets, displaying a significant increase in corrosion inhibition efficiency (IE). The sample with 5%-LnK showed the highest IE in both Tafel polarization and Nyquist curves.

ELALO-ELnK composites

2.11. Composites based on ELALO and epoxidized kraft lignin (ELnK) were prepared. Cross-linking was achieved exclusively by UV radiation. For a better dispersion of lignin, SDA (structure directing agents) were used. The ELALO-ELnK composites were investigated by FTIR, GF, CA, WAD, SEM, DMA and TGA.

2.12. The best GF results were obtained when Span and HSA were used for the systems with 1% ELnK (samples F8 and F9), indicating a slightly positive influence of the use of SDA on the conversion of the epoxy ring under UV treatment. Increasing the proportion of ELnK leads to lower GF values, with the lignin particles acting as UV blockers.

2.13. CA results are in agreement with the calculated WAD, samples F3 (ELALO-Span) and F8 (ELALO-Span-1%ELnK) being the most hydrophobic materials. In this respect, the long C18 fatty acid chains of Span 60 proved to be an advantage.

2.14. The general behavior of ELALO-SDA-ELnK materials, as evidenced by DMA results and by the shape of the recorded thermograms, point to a homogeneous material. The presence of SDA seemed to contribute to that.

2.15. Among the samples with 1% ELnK, F8 (ELALO-Span-1%ELnK) appeared to have the best thermal stability, as indicated by TGA measurements. Although the samples with a higher proportion of ELnK (5%, F10-F12) showed improved thermal properties, the negative influence on epoxy ring opening (as reflected in GF values) was a significant drawback.

6. Selected literature

[31] Hibbert B. *Experimental design in chromatography: A tutorial review*. Journal of Chromatography B, **2012**, 910, 2-13.

[32] Ferreira S.L.C., Bruns R.E., Ferreira H.S., Matos G.D., David J.M., Brandao G.C., da Silva E.G.P., Portugal L.A., dos Reis P.S., Souza A.S. & dos Santos W.N.L. *Box-Behnken design: An alternative for the optimization of analytical methods – Review*. Anal. Chim. Acta, **2007**, 597, 179.

[39] Chira N., Todașcă C., Nicolescu A., Păunescu G. & Roșca S. *Determination of the technical quality indices of vegetable oils by modern physical techniques*. U.P.B. Sci. Bull., Series B, **2009**, Vol. 71, Iss. 4 (3-12).

[40] Bălănucă B., Lungu A., Hanganu A., Stan L.R., Vasile E. & Iovu H. *Hybrid nanocomposites based on POSS and networks of methacrylated camelina oil and various PEG derivatives*. Eur. J. Lipid Sci. Technol. **2014**, 116, 458–469.

[44] AOAC. *Acid value of fats and oils*. In Official methods of analysis (16th Ed.). Washington, DC: Association of Official Analytical Chemists, **1995**; 940.28.

[46] Nguetnkam J.P., Kamga R., Villiéras F., Ekodeck G.E. & Yvon J. *Assessing the bleaching capacity of some Cameroonian clays on vegetable oils*. Applied Clay Science, **2008**, 39, 113–121.

[47] Kreps F., Vrbikova L. & Schmidt S. *Influence of industrial physical refining on tocopherol, chlorophyll and beta-carotene content in sunflower and rapeseed oil*. Eur. J. Lipid Sci. Technol. **2014**, 116, 1572-1582.

[51] Salawudeen T.O., Arinkoola A.O., Jimoh M.O. & Akinwande B.A. *Clay Characterization and Optimisation of Bleaching Parameters for Palm Kernel Oil Using Alkaline Activated Clays*. Journal of Minerals and Materials Characterization and Engineering, **2014**, 2, 586-597.

[170] Ungureanu E., Trofin A.E., Ariton A.M., Jităreanu D.C., Ungureanu O., Gîlcă V., Borș S.I. & Popa V.I. *Applications of epoxidated lignins for bioprotection of lignocellulosic materials*. Cellulose Chem. Technol., **2016**, 50 (1), 77-85.

[180] Malutan T., Nicu R. & Popa V.I. *Lignin modification by epoxidation*. BioResources, **2008**, 3(4), 1371-1376.

[181] Bhattacharyya S., Matsakas L., Rova U. & Christakopoulos P. *Melt Stable Functionalized Organosolv and Kraft Lignin Thermoplastic*. Processes, **2020**, 8, 1108.

[189] Gosselink R.J.A., Snijder M.H.B., Kranenbarg A., Keijsers E.R.P., de Jong E. & Stigsson L.L. *Characterisation and application of NovaFiber lignin*. Industrial Crops and Products, **2004**, 20, 191–203.

[201] Dastpak A., Yliniemi K., Monteiro M.C.O., Höhn S., Virtanen S., Lundström M. & Wilson B.P. *From Waste to Valuable Resource: Lignin as a Sustainable Anti-Corrosion Coating*. Coatings, **2018**, 8, 454.

[224] https://polymerdatabase.com/polymer%20classes/Lignin%20type.html (accesat pe 3/07/2022)

[225] Patil C.K., Rajput S.D., Marathe R.J., Kulkarni R.D., Phadnis H., Sohn D., Mahulikar P.P. & Gite V.V. *Synthesis of bio-based polyurethane coatings from vegetable oil and dicarboxylic acids*. Prog. Org. Coat., **2017**, 106, 87–95.

[227] Wang S., Hu Z., Shi J., Chen G., Zhang Q., Weng Z., Wu K. & Lu M. *Green synthesis of graphene with the assistance of modified lignin and its application in anticorrosive waterborne epoxy coatings*. Appl. Surf. Sci., **2019**, 484, 759–770.

[231] Okesola B.O., Vieira V.M.P., Cornwell D.J., Whitelaw N.K. & Smitha D.K. *1,3:2,4-Dibenzylidene-D-sorbitol (DBS) and its derivatives - Efficient, versatile and industrially-relevant low-molecular-weight gelators with over 100 years of history and a bright future*. Soft Matter, **2015**,11, 4768-4787.
[232] Sadeghifar H. & Ragauskas A. *Lignin as a UV Light Blocker—A Review*. Polymers, **2020**, 12, 1134.
[233] Rogers M.A., Wright A.J. & Marangoni A.G. *Nanostructuring fiber morphology and solvent inclusions in 12-hydroxystearic acid / canola oil organogels*. Current Opinion in Colloid & Interface Science, **2009**, 14, 33–42.

7. Dissemination of results

Articles published in ISI rated journals:

1) **R.S. Komartin**, R. Stan, B. Bălănucă, N. Chira & A. Hanganu; *Treatment of the oil of Lallemantia iberica with activated adsorbents*. **U.P.B. Sci. Bull. Series B, 2019,** Vol. 81, Iss. 4.

2) **R.S. Komartin**, M. Stroescu, N. Chira, R. Stan & A. Stoica-Guzun; *Optimization of oil extraction from Lallemantia iberica seeds using ultrasound-assisted extraction*. **Food Measure, 2021,** 15**,** 2010–2020. https://doi.org/10.1007/s11694-020-00790-w (IF=3.006)

3) **R.S. Komartin**, B. Bălănucă, M.I. Necolau, A. Cojocaru & R. Stan; *Composite materials from renewable resources as sustainable corrosion protection coatings*. **Polymers, 2021,** 13, 3792. https://doi.org/10.3390/polym13213792 (IF=4.967)

4) The data obtained in ***Chapter 5.3.*** will be submitted for publication.

Papers presented at national and international conferences:

1) **R.S. Komartin**, N. Chira, B. Bălănucă, M. Raicopol & R. Stan; *Epoxidized Lallemantia iberica seed oil for novel ecofriendly composite materials*. 20st Romanian International Conference on Chemistry and Chemical Engineering, RICCCE 20, 6–9 September 2017, Poiana Brașov, România.

2) **R.S. Komartin**, B. Bălănucă, R. Stan & A. Hanganu; *Anti-corrosion coatings based on crosslinked epoxidized Lallemantia oil and lignin*. 21st Romanian International Conference on Chemistry and Chemical Engineering, RICCCE 21, 4-7 September 2019, Constanța-Mamaia, România.

3) **R.S. Komartin**, M. Stroescu, N. Chira, R. Stan & A. Stoica-Guzun; ***Lallemantia iberica seeds oil extraction***. International Chemical Engineering and Material Symposium, SICHEM 2020, 17-18 September 2020.

4) **R.S. Komartin**, B. Bălănucă, M. Necolau & R. Stan; *Epoxidized vegetable oil for anti-corrosion coatings.* 5th International Conference on Chemical Engineering, ICCE 2020, 28-30 September 2020, Iași, România.

5) **R.S. Komartin**, B. Bălănucă & R. Stan; *Composite materials from epoxidized linseed oil and lignin.* International Conference on Smart Materials & Material Engineering", ICSMME 2021, 28-29 September 2021, Lisabona, Portugalia.